Electronic structure and magnetism in Bi_2Te_3, Bi_2Se_3, and Sb_2Te_3 doped with transition metals (Ti–Zn)

P. Larson* and Walter R. L. Lambrecht
Department of Physics, Case Western Reserve University, 10900 Euclid Avenue, Cleveland, Ohio 44106, USA
(Received 8 July 2008; published 14 November 2008)

A less studied class of magnetic semiconductors based on the tetradymite structure compounds, which include Bi_2Te_3, Bi_2Se_3, and Sb_2Te_3, doped with 3*d* transition-metal (*T*) elements is investigated using the full-potential linearized muffin-tin orbital method in the local spin-density approximation (LSDA). The small size of the *T* atoms (Ti–Zn) relative to the larger Bi/Sb atom site leads to a strong lattice relaxation, which primarily affects the atoms close to the defect in neighboring layers but has less impact within the layer containing the *T* ion. Even with the relaxation, the size difference leads to quite localized 3*d* states and hence a high-spin state with large magnetic moments. The valence is 3+ for the first half of the series but reduces closer to 2+ (Co) or 1+ (Ni) for the latter half of the series. This reduction is due to hybridization in the transition-metal 3*d* state with the Se/Te *p* state of the atom in the layer closest to the *T* site which reduces the amount of charge transfer between these two atoms. It corresponds to a competition between the stabilization by the exchange energy dominating for the early *T* ions and the covalent bonding effects for the later ones. For Cu and Zn the trend reverses and the valency is between 2+ and 3+ with a small magnetic moment remaining for Cu but a negligible moment for Zn. LSDA+*U* calculations for the Fe-Ni atoms slightly change this balance of the two effects and promote higher valency and larger magnetic moment.

DOI: 10.1103/PhysRevB.78.195207 PACS number(s): 71.20.−b, 85.75.−d, 72.20.Pa, 75.50.Pp

I. INTRODUCTION

The emergence of the field of spintronics[1] has led to a search for new magnetic semiconductors. These include diluted magnetic semiconductors (DMSs), adding small concentrations of transition-metal atoms into nonmagnetic semiconductors to obtain a composite material with both magnetic and semiconducting properties. Most of these are based on low doping of traditional group-IV,[2] III-V,[3] or II-VI semiconductors,[4] but other classes of semiconductors are candidates for DMSs as well. One such class is the tetradymite structure materials, including Bi_2Te_3, Bi_2Se_3, and Sb_2Te_3, which have been used extensively for thermoelectric applications.[5] For thermoelectric applications, these materials are doped with nonmagnetic atoms to enhance electron or hole transport. However, dilute doping with magnetic atoms have shown ferromagnetic (FM) transitions at low temperatures.[6–13]

Recently, Bi_2Te_3 and related systems with dilute dopings of transition-metal *T* atoms (Ti, V, Cr, Mn, and Fe) have been found to have ferromagnetic transitions at low temperatures. $Sb_{2-x}V_xTe_3$ was found to have a Curie temperature (T_C) around 22 K for $x\sim0.03$ (Refs. 6 and 7) while $Sb_{2-x}Cr_xTe_3$ was found to have a T_C around 20 K for $x\sim0.095$.[8] $Bi_{2-x}Mn_xTe_3$ orders around 10 K and $Sb_{2-x}Mn_xTe_3$ around 17 K, both for $x\sim0.02$,[9] though earlier measurements for $Sb_{2-x}Mn_xTe_3$ found no magnetic transition.[10] $Bi_{2-x}Fe_xTe_3$ orders around 12 K for $x\sim0.08$, but no transition is found above 2 K for $Bi_{2-x}Fe_xSe_3$ (Ref. 11) or $Sb_{2-x}Fe_xTe_3$.[13] However, the most significant interest in this class of materials comes from much larger dopings of thin films of $Sb_{2-x}V_xTe_3$, around $x\sim0.35$ which increases T_C to around 177 K and $Sb_{2-x}Cr_xTe_3$ and around $x\sim0.59$ which increases T_C to around 189 K.[8] Further increase with higher concentrations seems possible.[14] This is in line with the T_C of more traditional diluted magnetic semiconductors [~100 K (Ref. 15)], but no theoretical understanding of the magnetic properties yet exists.

This work will study the magnetic properties of dilute-doped Bi_2Te_3, Bi_2Se_3, and Sb_2Te_3 using electronic structure calculations. While the electronic structure of the pure compounds has been studied in detail,[16–22] the magnetic properties of the doped systems have not yet been investigated. We will investigate the larger doping levels corresponding to the larger values of T_C because they require smaller unit cells. This should allow us to obtain at least a qualitative understanding of the mechanisms leading to magnetism. In fact, we will show that even in the fairly small unit cells the *T* atoms interact only weakly magnetically, so the fundamental physics will remain unchanged even for the lower doping levels relevant to many of the experiments.

Bi_2Te_3, Bi_2Se_3, and Sb_2Te_3 doped with nonmagnetic atoms currently serve as the most important room-temperature thermoelectric materials available.[5] For this reason, the electronic structure of the pure compounds especially Bi_2Te_3 has been studied extensively in the past. While Shubnikov-de Haas and de Haas–van Alphen experiments find sixfold degenerate conduction and valence-band extrema in Bi_2Te_3,[23–25] several electronic structure calculations by different authors[17–20,22] have disagreed about the details near the Fermi level which are needed to determine the thermoelectric transport. Fewer studies have been done on Sb_2Te_3,[20,21] which can thus far only be grown *p* type[26,27] and Bi_2Se_3,[20] which can only be grown *n* type:[28,29] both having sixfold degenerate extrema. However, these details are not important to understand the magnetic properties of DMS Bi_2Te_3:*T* and related systems. The transition-metal atoms which have previously been studied (V, Cr, Mn, and Fe), unlike dopants used for thermoelectric applications (SbI_3, CuBr, excess Te,[30] etc.), have an unfilled 3*d* shell unlike the

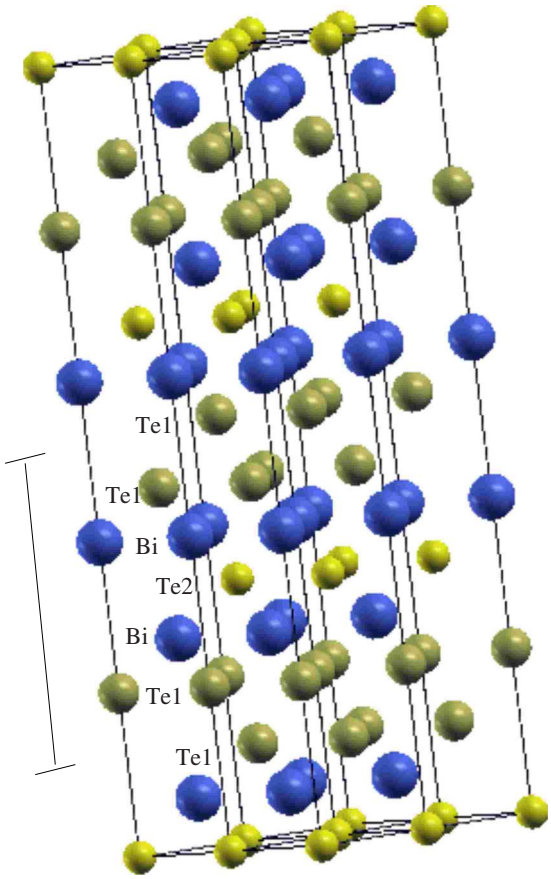

FIG. 1. (Color online) Crystal structure of Bi_2Te_3 (and related compounds). Large blue spheres Bi, small yellow Te_2, and larger greenish spheres Te_1. The five-atom "quintuple layer leaves" are separated by a van der Waals gap.

$5p$ states in Sb or $6p$ states in Bi. Since the transition-metal atoms have only partially filled $3d$ states, the bonding will differ significantly, so the nature of the bonding and the position of the $3d$ state are most important to understand the ferromagnetism.

II. CRYSTAL STRUCTURE AND METHOD

Bi_2Te_3, Sb_2Te_3, and Bi_2Se_3 form in the tetradymite crystal structure with the smallest unit cell having three inequivalent atoms in the rhombohedral (R-$3m$, No. 166) structure with Bi in the $2c$, Te_1 in the $2c$, and Te_2 in the $1a$ Wyckoff positions. The crystal structure consists of alternating layers of Bi and Te in the order Te_1-Bi-Te_2-Bi-Te_1 to form "quintuple layer leaves" with each atom in a roughly octahedral coordination with its neighbors (Fig. 1). Strong covalent bonding is seen within and between the layers, except for Te_1 (Se_1) which lies along a van der Waals gap across from another Te_1 (Se_1) atom. The positions of the atoms in this D_{3d}^5 symmetry are that all atoms lie along the trigonal axis. Te_2/Se_2 ($1a$) lies at the origin while the Bi/Sb($2c$) atoms lie at $\pm u$ ($0<u<1$) and the Te_1/Se_1($2c$) atoms lie at $\pm v$ ($0<v<1$). The experimental values of u and v used in the calculation are $u=0.399$ and $v=0.792$ for Bi_2Te_3 and Bi_2Se_3 with $u=0.4$ and $v=0.788$ for Sb_2Te_3. The experimental lattice constants for Bi_2Te_3 are $a=4.38$ Å and $c=30.5$ Å, for Bi_2Se_3 are $a=4.14$ Å and $c=28.6$ Å, and for Sb_2Te_3 are $a=4.25$ Å and $c=30.4$ Å when describing the axes in hexagonal coordinates.[31] These positions are relaxed in the 15-atom supercell described later in the paper.

Electronic structure calculations were carried out within the local spin-density approximation (LSDA) to density-functional theory (DFT) (Ref. 32) using a full-potential linear muffin-tin orbital (FP-LMTO) program[33] using the exchange-correlation parametrization of Barth and Hedin[34] for the spin-polarized case and that of Hedin and Lundqvist[35] in the non-spin-polarized case. This method uses an optimized basis set consisting of muffin-tin orbitals with smoothed Hankel functions as envelope functions. This program includes calculation of the atomic forces for the purpose of structural relaxation by a conjugate gradient method. The smoothing radii and κ values (Hankel function decay parameters) were carefully adjusted to optimize an efficient basis set with one s, p, and d state on each Sb, Te, Se, and T site and one s, p, d, and f state on each Bi site. The smooth interstitial quantities are calculated using a fine Fourier-transform mesh and the Brillouin-zone integrations were carried out with a well-converged k mesh based on a uniform division of reciprocal space. The details of the k-mesh integration depend on the size of the unit cell and will be discussed later in the paper.

III. RESULTS

A. Pure compound density of states

The band structures of Bi_2Te_3, Bi_2Se_3, and Sb_2Te_3 have been studied extensively[16–22] due to their importance as room-temperature thermoelectric materials. The density of states (DOS) for the pure system Bi_2Te_3, Bi_2Se_3, and Sb_2Te_3 is given in Fig. 2. The $Te(Se)_1$ and $Te(Se)_2$ $5(4)p$ states form below the Fermi level with the $5(4)s$ states around -10 eV. The Bi(Sb) $6(5)p$ states form above the Fermi level with significant hybridization only occurring within $\sim$0.1 eV of E_F itself. The covalent bonding leads to each Bi(Sb) in a 3+ state and each Te(Se) in a 2− state. Spin-orbit (SO) effects increase the hybridization and reduce the band gap in Bi_2Te_3 and Bi_2Se_3.[17–20] Sb_2Te_3 without spin orbit is a weak semimetal within LSDA or generalized gradient approximation (GGA) calculations (for the experimental lattice parameters); spin-orbit opening is a small gap due to the Sb $5p$-Te $5p$ hybridization.[20,21] The results shown here include spin-orbit coupling.

B. Basic DOS features

Experimental evidence shows that the transition-metal atoms replace the larger Bi(Sb) atoms within the lattice rather than Te(Se).[6,7,9,11,12] Calculations have been performed on SbTTe$_3$ (T=Ti-Zn, x=1). In these calculations, a $5\times5\times5$ mesh was used for the k points along with a real space $10\times10\times60$ mesh. SO interaction was included in the calculation, though little effect was seen on the magnetic properties. In the larger unit cells, SO was not included for this reason and to help speed convergence. Calculations were also per-

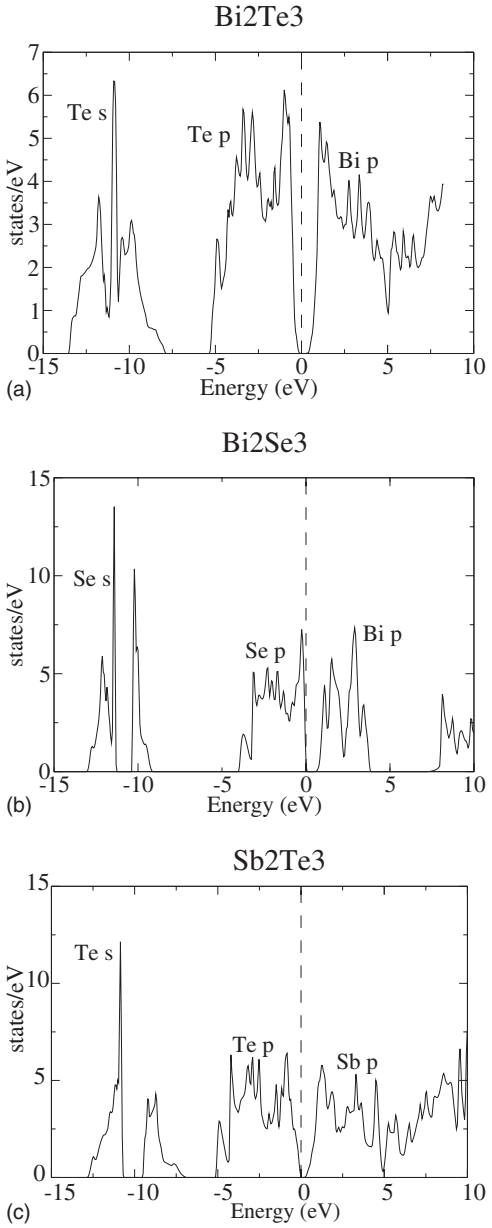

FIG. 2. Calculated total DOS for (a) Bi_2Te_3, (b) Bi_2Se_3, and (c) Sb_2Te_3. The states lying above the Fermi level (E_F) are Bi(Sb) 6(5)p, those just below E_F are $Te(Se)_1$ and $Te(Se)_2$ 5(4)p with the $Te(Se)_1$ and $Te(Se)_2$ 5(4)s lying near −10 eV.

formed using the hexagonal supercell containing 15 atoms (Fig. 1) with one Sb or Bi atom replaced by a T atom. This effectively changes x in $(Sb:Bi)_{2-x}T_x(Se:Te)_3$ from 1 to 0.333; the value in $Sb_2Te_3:V$ which has a T_C of 177 K.[14] In these calculations, a $3\times3\times3$ mesh was used for the k points along with a real space $60\times60\times180$ mesh.

The concentration of T in SbTTe$_3$ or BiTTe$_3$ is much higher than realized experimentally, so calculations are performed at this concentration only to understand the position of the T d states with respect to the DOS of Sb_2Te_3 and Bi_2Te_3. In the DOS of $SbVTe_3$ and $BiMnTe_3$, the transition-metal peaks are obscured by the Bi(Sb) and Te portions of the DOS; but the spin-majority (dotted lines) and spin-minority bands (dashed lines) corresponding to the

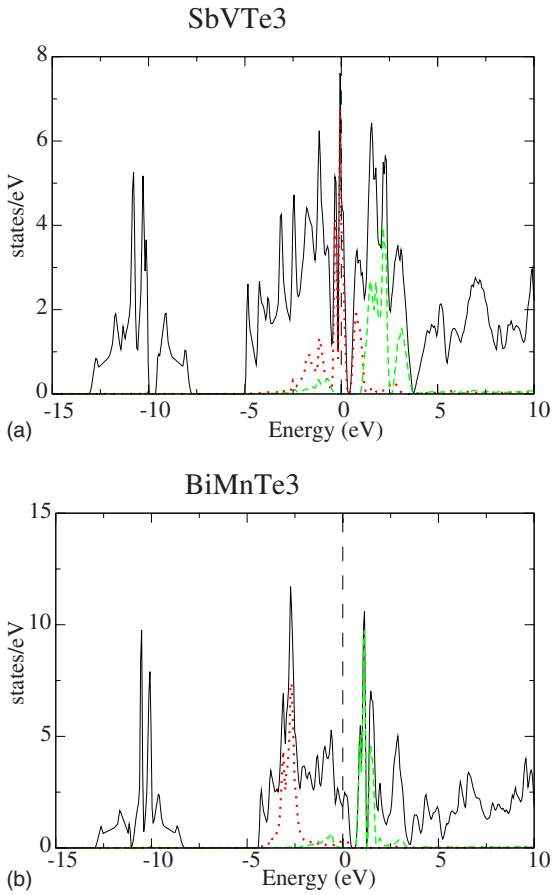

FIG. 3. (Color online) Calculated total DOS (black solid lines) for (a) $SbVTe_3$ and (b) $BiMnTe_3$. The transition-metal spin-majority partial density of states (PDOS) (red dotted lines) and spin-minority PDOS (green dashed lines) are narrow even for this concentration.

transition-metal 3d states (Fig. 3) lie above and below E_F. The nearest-neighbor environment of the Mn is approximately octahedral. In reality it has C_{3v} symmetry with three anions above and three below it. Yet, we do not see any splitting of the d states in t_{2g}- and e_g-like states but only a strong spin splitting. This means that the electronic structure is close to the atomic limit in which Hund's rules dictate maximum spin. While these states are narrow and lie separated into spin-minority states mostly above E_F and spin-majority states either partially filled or below E_F, there exists some hybridization between the transition-metal d states and the Te p and Bi/Sb p states. However, the layered structure and the size mismatch between the transition metal and the Bi/Sb site it replaces makes the hybridization fairly weak and does not affect the position of the transition-metal d state. The position is determined by the filling of the d states with 3+ valence.

C. Structural relaxation

The small transition-metal atom enters the larger Bi/Sb site which causes relaxation of the lattice. The latter was studied by minimizing the energy both as function of lattice

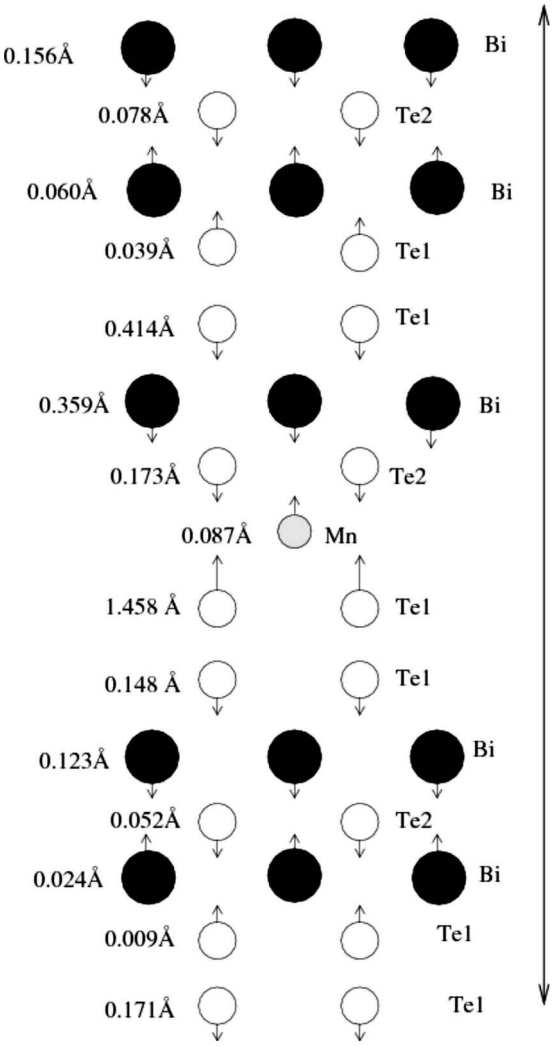

FIG. 4. Schematic diagram of the relaxation of Bi_5MnTe_9. One Te atom lying close to the smaller Mn atom moves considerably due to the difference in atomic radii of Mn and Bi which it replaces. The other atoms show little relaxation. The numbers indicate the amount of relaxation.

parameters and internal coordinates for the 15-atom-hexagonal unit cell. The Bi atom has an atomic radius of about 2.8 a.u. and Sb of about 2.6 a.u. compared to the typical size of the T atom (2.4 a.u.), all in their uncharged state. Some general features of the relaxation are noted. The atoms move more in Bi_2Te_3 and Bi_2Se_3 than in Sb_2Te_3 during relaxation, most likely caused by the slightly smaller Sb radius compared to that of Bi where the T atom is replaced.

The T atoms replace Bi(Sb) which lies between two Te(Se) atoms. Relaxation of the lattice parameters found these neighboring atoms moving to accommodate the smaller radius of the T atom, but the remaining atoms see a much smaller change in order to maintain the original crystal structure. An example of this relaxation is shown in the schematic of Bi_5MnTe_9 (Fig. 4). One Te atom lying next to Mn shifts significantly toward Mn to fill in the space left from the larger Bi atom. However, the relaxation of the rest of the lattice is fairly small, so that the rest of the lattice remains very similar to that of the undoped compound.

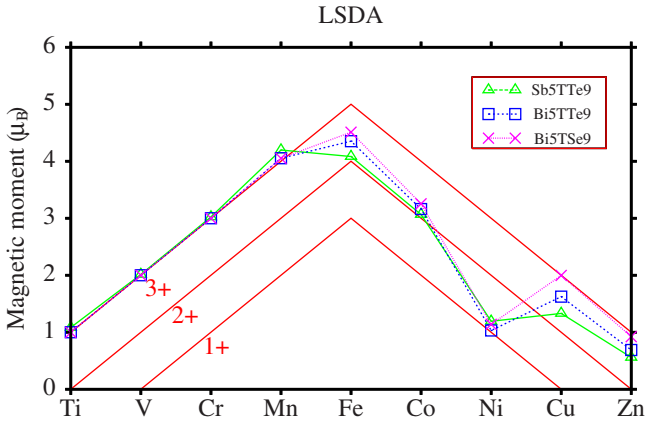

FIG. 5. (Color online) Calculated moments using LSDA for Sb_5TTe_9, Bi_5TTe_9, and Bi_5TSe_9 for T from Ti to Zn. The upper curve corresponds to a valence of 3+, the middle to a valence of 2+, and the lowest to a valence of 1+.

D. Magnetic moments

A simple picture of the T moment in Bi_2Te_3:T and related compounds is obtained by considering that the valence of the T should be 3+; the same as the Bi or Sb atom that it replaces ($Bi_2^{3+}Te_3^{2-}$). Calculations of the magnetic moment of the 15 atom supercell found that the moments are near integer for Ti to Cr, but for Mn and Fe calculations fall below the curve to about 2+ then down to about 1+ for Ni while for Cu and Zn the values lie between 2+ and 3+ valence (Fig. 5). The occurrence of integer moments is also closely related to half-metallic behavior.[36–38] As shown in Sec. III E below, the early T shows a gap in their minority spin for the ferromagnetic state and thus half metallic.

In order to understand the magnetism and position of the transition-metal d states, the PDOS has been plotted across the series from T=Ti to Zn in Sb_5TTe_9. In Sb_5TiTe_9 [Fig. 6(a)] the spin-minority states become hybridized with the Sb p states above E_F while all five spin-majority states become pinned at E_F so that one electron is filled consistent with 3+ valence. A similar situation is seen in Sb_5VTe_9 [Fig. 6(b)] with the spin-majority state slightly lower to accommodate two electrons. In Sb_5CrTe_9 [Fig. 6(c)] the d states split with three electrons hybridizing with the Te p states between −1 and −4 eV with a much narrower peak at E_F. This situation continues in Sb_5MnTe_9 [Fig. 6(d)] which appears to have a fairly wide splitting of the spin-majority states below E_F and the spin-minority states above. The Fe d majority states in Sb_5FeTe_9 [Fig. 6(e)] become pinned at E_F but still yield a moment which is close to that of 3+.

Up to this point, as seen in Fig. 5, the transition-metal state produces a moment consistent with a 3+ configuration. The situation changes for Sb_5CoTe_9 [Fig. 6(f)] with a valence of about 2+. In Sb_5NiTe_9 [Fig. 6(g)] the valence reduces to 1+ as the minority-spin states move below E_F and hybridize with the Te p states. Ni-doped Sb_2Te_3 has not been investigated for DMS materials, but these calculations predict significantly different behavior than that of V, Cr, Mn, and Fe which have been studied so far. The valence of Sb_5CuTe_9 [Fig. 6(h)] lies much closer to 3+ where there

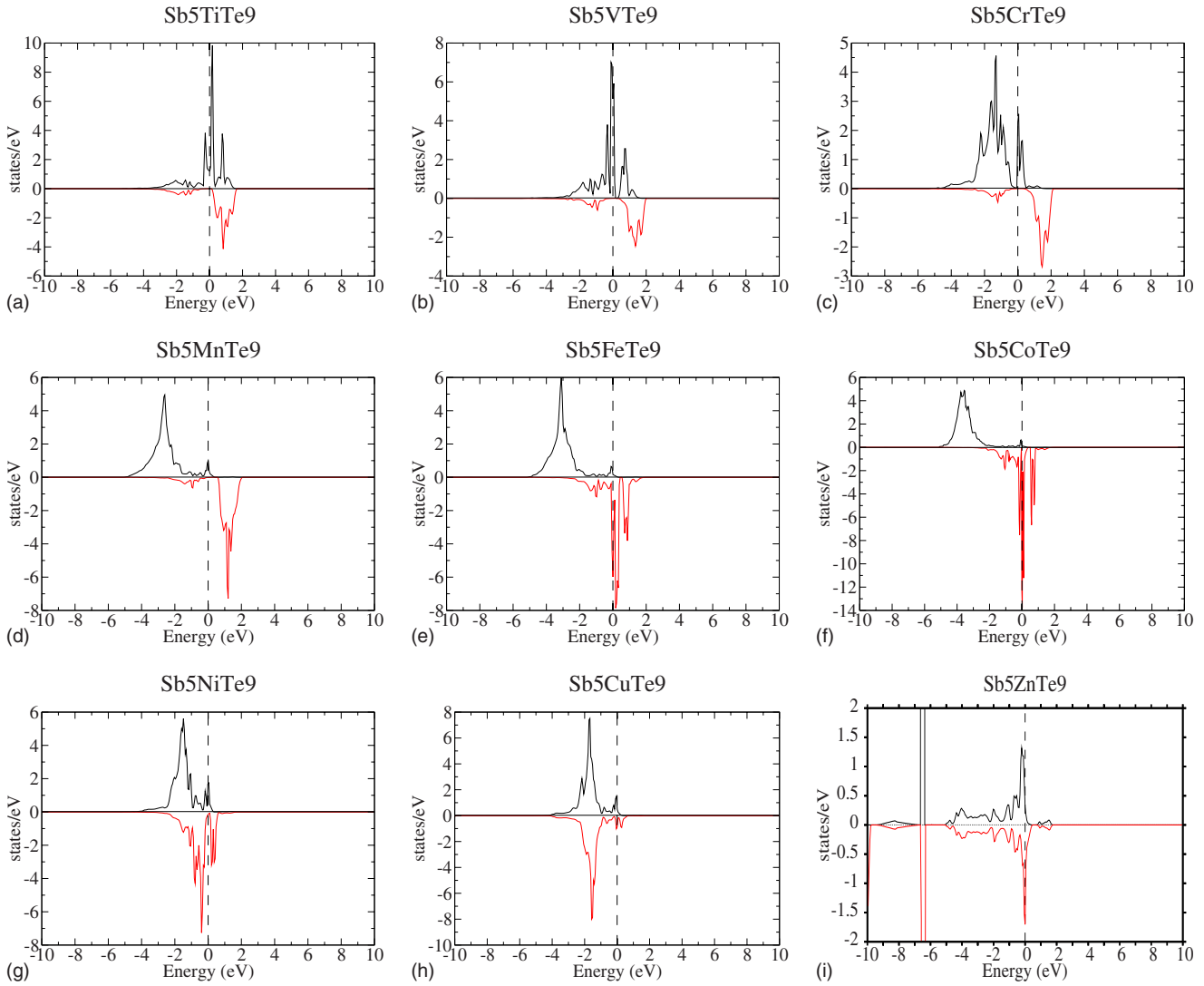

FIG. 6. (Color online) Calculated partial DOS T $3d$ for Sb_5TTe_9 and for T from Ti to Zn. Spin-majority states are shown positive while spin-minority states are plotted negative.

exists only a small remnant of the spin-minority state which gives the magnetic moment, the remaining bands hybridized with Te p below E_F. In Sb_5ZnTe_9 [Fig. 6(i)] we see truly localized atomiclike states near where the small moment arises from states near E_F.

We may explain this trend as follows: In the early T ions Hund's rules provide a significant stabilization because of the exchange energy. When we go beyond half filling of the d shell, however, the magnetic stabilization effect is decreased and covalent bonding starts to take over. In the Fe, Co, and Ni cases, the minority-spin states become clearly split in two peaks (t_{2g}- and e_g-like states) and the lower of these (the t_{2g}) tends to shift down below the Fermi energy to lower the band-structure energy. This results in a reduction in the valency and with it an increase in the size of the ion to better fit the Bi or Sb location. By the time we reach Cu, a 1+ ion would have corresponded to a d^{10} nonmagnetic configuration. Apparently, it is more favorable to still obtain some stabilization from the exchange effect by reversing the trend and going back to a slightly more than 2+ ion and more so in the Bi (more space less covalency) case than in the Sb case. This is because the d states now already lie rather deep and do not hybridize as efficiently with the anion p states anymore. Thus, it appears that the minimization of the energy requires a careful compromise between the magnetic exchange energy stabilization and adjusting the size of the ion to promote covalent bonding stabilization.

To further illustrate this point, we compare in more detail the partial DOS of Sb_5MnTe_9 and Sb_5NiTe_9 in Fig. 7. In particular, we here show the T d and the Te p PDOS of the Te atom closest to the T atom. This atom, as noticed earlier, moves even closer to the T atom by relaxation and thus reinforces the effect discussed here. In the early T element Mn, we see almost no overlap between the Te p states and the empty Mn d states with the Te p states almost completely filled, corresponding to close to ionic bonding where Te is a 2− ion and Mn a 3+ ion. For Ni, however, we see a substantial hybridization of empty Ni d and empty Te p states. This means that the ionicity is reduced. There is a competition between the energy gain in filling the Ni d states and the Te p states and the system prefers to leave the Te p states partially unoccupied by filling the Ni d states instead. In par-

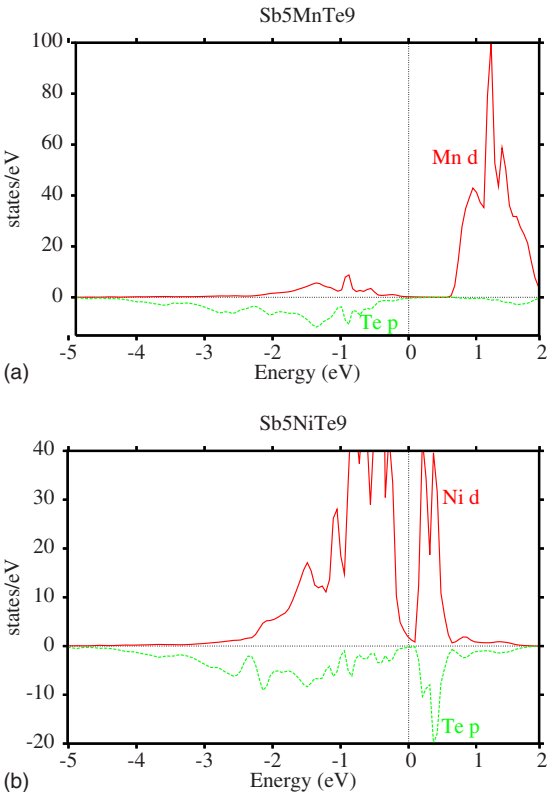

FIG. 7. (Color online) Calculated DOS for (a) Mn d states (positive) and (b) Ni d states (positive) and p states of the nearest Te atom (negative) for (a) Sb_5MnTe_9 and (b) Sb_5NiTe_9. The empty Ni d states interact strongly with the Te p states while the Mn d states do not.

ticular there is a large overlap between Ni d_{xy} and $d_{x^2-y^2}$ states and Te p_y states, as allowed in C_{3v} symmetry.

E. Exchange coupling of magnetic moments

Our electronic structure calculations confirm the existence of a ferromagnetic ground state in these materials. A 30 atom supercell was constructed by doubling the relaxed 15 atom unit cell along the x axis to make $Sb_{10}V_2Te_{18}$. The FM state has lower energy than the antiferromagnetic (AFM) state by 0.15 eV/T atom. The V d states in the FM configuration (Fig. 8) lie above those in the AFM configuration in the conduction band with the peak in the conduction band just below E_F sharper for the FM case than for the AFM case. The value of the d level DOS crossing of that crosses E_F is around 3 states/eV/cell for the AFM case and 2 states/eV/cell for the FM case. Another important point to note is that the spin-minority band in the FM phase has a gap in the spectrum at E_F in the presence of the large spin-majority peak (Fig. 8) while no gap occurs in the AFM phase. A similar gap in the spin-minority band in the FM phase can be seen for Sb_5TiTe_9, Sb_5VTe_9, and Sb_5MnTe_9 [Figs. 6(a), 6(b), and 6(d)].

F. LSDA+U calculations

As seen up to this point, the nature of the ferromagnetic moment is understood for doping with most of the early

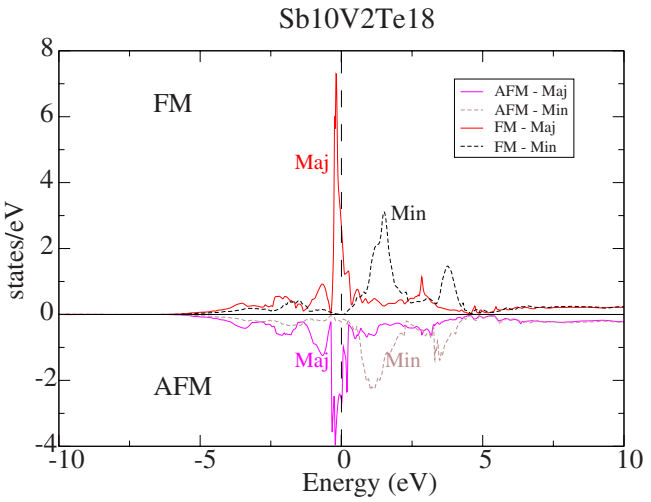

FIG. 8. (Color online) Partial DOS for V 3d for $Sb_{10}V_2Te_{18}$ in both the FM (positive) and AFM states (negative). The spin-majority states are solid (red for FM, pink for AFM) lines while the spin-minority states are dashed (black for FM, brown for AFM case).

transition-metal elements and the very late ones, but the moments for Fe, Co, and Ni are smaller than expected. The transition-metal T atoms in the larger Bi(Sb) sites are expected to have the same valence (3+) as the atom it replaces. This is what is seen for T from Ti to Mn and to a lesser extent for Cu-Zn, but Fe, Co, and Ni have a magnetic moment which corresponds to a 2+ or 1+ valence (Fig. 5). The T d states for Fe, Co, and Ni appear to be fixed at the Fermi level due to partial filling. It is possible that this is an artifact of the LSDA which tends to underestimate magnetic moments in some cases. We thus investigate whether the LSDA+U approach[39,40] may result in a shifting of the d states away from E_F and thus restoring the 3+ valency. We use the LSDA+U approach for the latter half of the transition-metal series as recently implemented in the FP-LMTO approach.[41] LSDA+U adds a Hubbard U correction to specific orbitals in order to add many-body physics to LSDA density-functional calculations. Additional orbital-dependent effects of partially filled shells are described by J. Typical values for U of 8 eV and J of 1 eV were used to shift the T d orbitals. The filled d states move down in energy while the empty d states move to higher energies. The values of the magnetic moment obtained in this approach are given in Fig. 9.

While the Fe d orbitals are moved away from E_F to yield a $5\mu_B$ moment (3+valence), the effect is smaller for Co-Zn. Bi_5CoTe_9 is found to have a moment of $4\mu_B$ (3+valence), but Sb_5CoTe_9 and Bi_5CoSe_9 have moments closer to $3\mu_B$. For all three materials doped with Ni, the moment increases from the LSDA value of $1\mu_B$ but falls below $2\mu_B$. The moments are nearly the same for all three compounds with Cu and Zn dopings. These results are consistent with the above observation that a subtle balance between tendencies for covalency and magnetism is at work for the later transition elements and with a slight increase in the tendency toward magnetism using the LSDA+U functional.

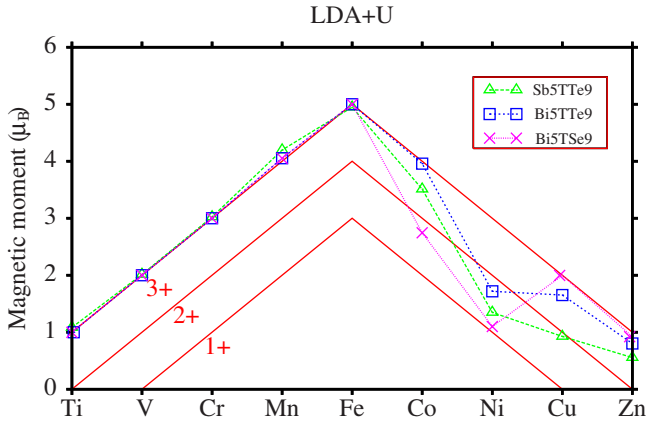

FIG. 9. (Color online) Calculated moments using LSDA+U for Sb_5TTe_9, Bi_5TTe_9, and Bi_5TSe_9 for T from Ti to Zn. The upper curve corresponds to a valence of 3+, the middle to a valence of 2+, and the lowest to a valence of 1+.

IV. SUMMARY

Electronic structure calculations have found that the transition-metal (T=Ti,V,Cr,Mn,Fe,Co,Ni,Cu,Zn)-doped tetradymite compounds $Bi_{2-x}T_xTe_3$, $Bi_{2-x}T_xSe_3$, and $Sb_{2-x}T_xTe_3$ arise from filling of the 3d bands. All of the atoms move closer to the smaller T site, but the Te atoms in neighboring layers relax around the transition-metal defect with the relative positions of the other layers mostly unchanged. The spin-majority and spin-minority bands hybridize only weakly with the Bi/Sb p and Te/Se p states. The weak hybridization leads to an almost atomic configuration dominated by Hund's rule stabilization of the maximum spin for the T^{3+} ions up to half filling of the d shell with barely any splitting of the T d states noticeable. For Co and Ni, however, the magnetic exchange stabilization is weaker and instead a more covalent solution is found indicated by a splitting of the minority-spin d states in two peaks; a preference for 2+ valency with a larger ion and hence a reduced magnetic moment. This is primarily due to a competition between filling the Te p states of the nearest-neighbor Te of the T ion and the energy gain from filling one of the split T d states. For Cu and Zn, the trend reverses again to a valency between 3+ and 2+. LSDA+U calculations favor the magnetic stabilization and, in particular for Fe, shift the d states below the Fermi level, thereby restoring an integer valency (3+) and magnetic moment. They also tend to increase the valency and magnetic moment slightly for Co and Ni but do not completely restore the ideal valency of 3+ for the tetradymite cation. The ferromagnetic coupling between these localized magnetic moments is found to be preferred over the antiferromagnetic coupling.

ACKNOWLEDGMENTS

This work was supported by the Office of Naval Research under Grant No. N00014-02-1-0880. Calculations were performed using resources of the Ohio Supercomputer Center.

*Present address: Department of Physics and Astronomy, University of Nebraska, Lincoln, NE 68588.

[1] S. A. Wolf, D. D. Awschalom, R. A. Buhrman, J. M. Daughton, S. von Molnar, M. L. Roukes, A. Y. Chtchelkanova, and D. M. Treger, Science **294**, 1488 (2001).
[2] Y. D. Park, A. T. Hanbicki, S. C. Erwin, C. S. Hellberg, J. M. Sullivan, J. E. Mattson, T. F. Ambrose, A. Wilson, G. Spanos, and B. T. Jonker, Science **295**, 651 (2002).
[3] H. Ohno, Science **281**, 951 (1998); Y. Ohno, D. K. Young, B. Beschoten, F. Matsukura, H. Ohno, and D. D. Awschalom, Nature (London) **402**, 790 (1999); H. Ohno, Science **291**, 840 (2001).
[4] R. D. McNorton, T. M. Schuler, J. M. MacLaren, and R. A. Stern, Phys. Rev. B **78**, 075209 (2008).
[5] *Thermoelectric Materials 2003-Research and Applications*, MRS Symposia Proceedings No. 793, edited by G. S. Nolas, J. Yang, T. P. Hogan, and D. C. Johnson (Materials Research Society, Pittsburgh, 2003).
[6] J. S. Dyck, W. Chen, P. Hájek, P. Lošt'ák, and C. Uher, Physica B **312-313**, 820 (2002).
[7] J. S. Dyck, P. Hájek, P. Lošt'ák, and C. Uher, Phys. Rev. B **65**, 115212 (2002).
[8] J. S. Dyck, C. Drasar, P. Lošt'ák, and C. Uher, Phys. Rev. B **71**, 115214 (2005).
[9] J. Choi, S. Choi, J. Choi, Y. Park, H. M. Park, H. W. Lee, B. C. Woo, and S. Cho, Phys. Status Solidi B **241**, 1541 (2004).
[10] J. S. Dyck, P. Svanda, P. Lošt'ák, J. Horak, W. Chen, and C. Uher, J. Appl. Phys. **94**, 7631 (2003).
[11] V. A. Kulbachinskii, A. Yu. Kaminskii, K. Kindo, Y. Narumi, K. Suga, P. Lošt'ák, and P. Svanda, Physica B **311**, 292 (2002); V. A. Kulbachinskii, A. Yu. Kaminskii, V. G. Kytin, and A. de Visser, J. Magn. Magn. Mater. **272-276**, 1991 (2004).
[12] J. Horak, P. C. Quayle, J. S. Dyck, C. Drasar, P. Lošt'ák, and C. Uher, J. Appl. Phys. **103**, 013516 (2008).
[13] Z. Zhou, M. Zabéík, P. Lošt'ák, and C. Uher, J. Appl. Phys. **99**, 043901 (2006).
[14] Z. Zhou, Yi-J. Chien, and C. Uher, Appl. Phys. Lett. **87**, 112503 (2005).
[15] H. Ohno, J. Magn. Magn. Mater. **200**, 110 (1999).
[16] G. A. Thomas, D. H. Rapke, R. B. Van Dover, L. F. Mattheis, W. A. Surden, L. F. Schneemaper, and J. V. Waszczak, Phys. Rev. B **46**, 1553 (1992).
[17] S. K. Mishra, S. Satpathy, and O. Jepsen, J. Phys.: Condens. Matter **9**, 461 (1997).
[18] P. Larson, S. D. Mahanti, and M. G. Kanatzidis, Phys. Rev. B **61**, 8162 (2000).
[19] S. J. Youn and A. J. Freeman, Phys. Rev. B **63**, 085112 (2001).
[20] P. Larson, Phys. Rev. B **68**, 155121 (2003).
[21] T. Thonhauser, T. J. Scheidemantel, J. O. Sofo, J. V. Badding, and G. D. Mahan, Phys. Rev. B **68**, 085201 (2003).
[22] M. Kim, A. J. Freeman, and C. B. Geller, Phys. Rev. B **72**, 035205 (2005).

[23] H. Köhler, Phys. Status Solidi B **73**, 95 (1976); **74**, 591 (1976).
[24] J. R. Drabble, R. D. Grooves, and R. Wolfe, Proc. Phys. Soc. London **71**, 430 (1958).
[25] L. R. Testardi, P. J. Stiles, and E. Burnstein, Solid State Commun. **1**, 28 (1963).
[26] A. von Middendorff, K. Dietrich, and G. Lanwehr, Solid State Commun. **13**, 443 (1973).
[27] I. V. Gasenkova, L. D. Ivanova, and Yu. V. Granatkina, Inorg. Mater. **37**, 1112 (2001).
[28] L. Tichy and J. Horak, Phys. Rev. B **19**, 1126 (1979).
[29] V. A. Kulbachinskii, N. Miura, H. Nakagawa, H. Arimoto, T. Ikaida, P. Lošt'ák, and C. Drasar, Phys. Rev. B **59**, 15733 (1999).
[30] D. B. Hyun, J. S. Hwang, B. C. You, T. S. Oh, and C. W. Hwang, J. Mater. Sci. **33**, 5595 (1998); C. W. Hwang, D. B. Hyun, H. P. Ha, and T. S. Oh, *ibid.* **36**, 3291 (2001).
[31] R. W. G. Wyckoff, *Crystal Structures* (Krieger, Melbourne, FL, 1986), Vol. 2.
[32] P. Hohenberg and W. Kohn, Phys. Rev. **136**, B864 (1964); W. Kohn and L. J. Sham, *ibid.* **140**, A1133 (1965).
[33] M. Methfessel, M. van Schilfgaarde, and R. A. Casali, in *Electronic Structure and Physical Properties of Solids: The Uses of the LMTO Method*, Springer Lecture Notes, Workshop Mont Saint Odille, France, 1998, edited by Hughes Dreysse (Springer, Berlin, 2000), pp. 114–147.
[34] U. von Barth and L. Hedin, J. Phys. C **5**, 1629 (1972).
[35] L. Hedin and B. I. Lundqvist, J. Phys. C **4**, 2064 (1971).
[36] I. Galanakis, Ph. Mavropoulos, and P. H. Dederichs, J. Phys. D **39**, 765 (2006).
[37] M. S. Miao and W. R. L. Lambrecht, Phys. Rev. B **72**, 064409 (2005).
[38] M. S. Miao and Walter R. L. Lambrecht, Phys. Rev. B **71**, 064407 (2005).
[39] V. I. Anisimov, J. Zaanen, and O. K. Andersen, Phys. Rev. B **44**, 943 (1991); V. I. Anisimov and O. Gunnarsson, *ibid.* **43**, 7570 (1991); V. I. Anisimov, F. Aryasetiawan, and A. I. Lichtenstein, J. Phys.: Condens. Matter **9**, 767 (1997).
[40] A. I. Liechtenstein, V. I. Anisimov, and J. Zaanen, Phys. Rev. B **52**, R5467 (1995); S. L. Dudarev, G. A. Botton, S. Y. Savrasov, C. J. Humphreys, and A. P. Sutton, *ibid.* **57**, 1505 (1998).
[41] P. Larson, W. R. L. Lambrecht, A. Chantis, and M. van Schilfgaarde, Phys. Rev. B **75**, 045114 (2007).